

Article

First Principles Calculation of the Stability of Iron Bearing Carbonates at High Pressure Conditions

Jun Tsuchiya ^{1,2,*} , Risa Nishida ^{1,†} and Taku Tsuchiya ^{1,2,†} 

¹ Geodynamics Research Center (GRC), Ehime University, Ehime 790-8577, Japan; soranotumiki@outlook.jp (R.N.); tsuchiya.taku.mg@ehime-u.ac.jp (T.T.)

² Earth-Life Science Institute (ELSI), Tokyo Institute of Technology, Tokyo 152-8550, Japan

* Correspondence: junt@ehime-u.ac.jp

† These authors contributed equally to this work.

Received: 16 October 2019; Accepted: 2 January 2020; Published: 8 January 2020



Abstract: Carbonate minerals such as ferromagnesite (Mg,FeCO_3) are suggested to be a possible major deep-carbon host in the lower mantle, because ferromagnesite is possibly stabilized by Fe spin crossover under pressure. However, the behavior of Fe-bearing carbonates under lower mantle pressure conditions has not been suitably examined thus far. Thus, in this study, we investigate the high-pressure stability of ferromagnesite and possible high-pressure structures with the chemical composition of $(\text{Mg}_{0.833}\text{Fe}_{0.167})\text{CO}_3$ via first principles calculation using internally consistent local density approximation with Hubbard parameter (LDA+U) method, which can more accurately account for the electronic state of Fe than the LDA and generalized gradient approximation (GGA) approaches. The enthalpy values obtained via our calculations suggest that $(\text{Mg}_{0.833}\text{Fe}_{0.167})\text{CO}_3$ undergoes phase transition from the $R\bar{3}c$ structure (high spin) to the $P\bar{1}$ (high spin) at 50 GPa, and to $C2/m$ (high-spin) structure above 80 GPa, under static 0 K conditions. Therefore, no spin transitions in these carbonate minerals is expected under the lower mantle pressure conditions.

Keywords: carbonate mineral; high pressure; first principles calculation

1. Introduction

Carbon is one of the important volatile elements in the Earth. Accordingly, it is known to significantly affect the climate as well as dynamics processes on the planet, such as volcanic activity. Carbon is primarily transported into deep Earth in the form of carbonate minerals, such as magnesite (MgCO_3), calcite and aragonite (CaCO_3), dolomite ($\text{CaMg}(\text{CO}_3)_2$), and siderite (FeCO_3) [1,2]. Among them, magnesite has attracted special attention from researchers because of its high stability under high pressure and temperature conditions in the Earth's interior [3–8]. However, in general, the circulation mechanism of carbon in the deep interior remains largely unknown [9,10].

High pressure and temperature experiments conducted in some previous studies using a diamond-anvil cell (DAC) found that magnesite did not undergo phase transformation at 80 GPa between temperatures of 2000–2500 K [3–5]. In contrast, through an in situ X-ray diffraction experiment conducted in a later work, it was shown that magnesite transformed into an unknown form at ~ 115 GPa and 2100–2200 K [7]. Recently, in a study wherein in situ X-ray diffraction measurement using a double-sided laser-heated DAC was conducted, a phase transformation from magnesite to magnesite-II (space group $C2/m$) was reported at 80 GPa [8], which had previously been predicted based on ab initio calculations [11,12].

The structural evolution of magnesite under ultrahigh pressure conditions has been explored theoretically [11,12]. Oganov et al. [11] reported that the magnesite structure transformed to space group $C2/m$ with a lower enthalpy than that of magnesite above 82.4 GPa; this transformation was

predicted based on calculations performed using *ab initio* evolutionary crystal structure searching algorithm. In addition, they also reported that the $C2/m$ crystal structure transformed to one with space group $P2_1$ above 138 GPa. Pickard and Needs [12] also conducted *ab initio* random structure searching of the $MgCO_3$ system and found that its new crystal structure (space group $P\bar{1}$) has a lower enthalpy than that of the $C2/m$ phase in the range of 80–101 GPa.

The presence of Fe in carbonate minerals has been shown to modify their phase stability under high pressure and temperature conditions [13–15]. Ferromagnesite $(Mg,Fe)CO_3$ is a solid solution of magnesite and siderite. Several different results on the high pressure behaviors of ferromagnesite have been reported thus far. In particular, siderite-rich ferromagnesite $(Fe_{0.75}Mg_{0.25})CO_3$ has been reported to transform into a new Fe^{3+} -bearing high pressure carbonate, Fe_3O_4 magnetite, and nano-diamonds above 80 GPa and 1850–2300 K [2]. In contrast, it was found that $(Fe_{0.65}Mg_{0.35})CO_3$ transforms into an orthorhombic phase (phase II with space group $Pmm2$) above ~ 50 GPa and 1400 K; this was determined via a synchrotron X-ray diffraction experiment using a laser-heated DAC [14]. It should be noted that these previous experiments were strongly affected by the oxygen fugacity in the system at high pressure–temperature conditions [2,14,16].

Moreover, it has been suggested that spin crossover of Fe in high-pressure carbonate phases stabilizes them at relatively lower pressure conditions [14]. In particular, high-spin (HS) to low-spin (LS) transition of ferrous iron (Fe^{2+}) in $(Mg,Fe)CO_3$ ferromagnesite has been indicated via Raman spectroscopy, X-ray emission spectroscopy, and X-ray diffraction measurements at ~ 50 GPa [14,17–21]. In addition, first principles calculation by Hsu and Huang [22] showed that a spin transition from HS to LS occurs in ferromagnesite at around 45–50 GPa, which is consistent with the previously conducted experiments. Furthermore, Hsu and Huang [22] also found that spin transition pressure does not depend on the Fe concentration in ferromagnesite.

In general, it is believed that the spin transition of Fe significantly affects the structure, elasticity, and thermodynamic properties of minerals owing to a large difference between the ionic radii of Fe in its HS and LS states. However, these effects of Fe spin transitions on the stability of high-pressure phases of ferromagnesite have not been investigated thus far. Thus, in this study, we investigated the structure and stability of ferromagnesite and its possible high-pressure phases via first principles calculation. Because the strongly correlated nature of Fe cannot be properly reproduced using local density approximation (LDA) and generalized gradient approximation (GGA) approaches, we used the internally consistent LDA+U method wherein the Hubbard parameter U was determined based on our first principles calculation [23].

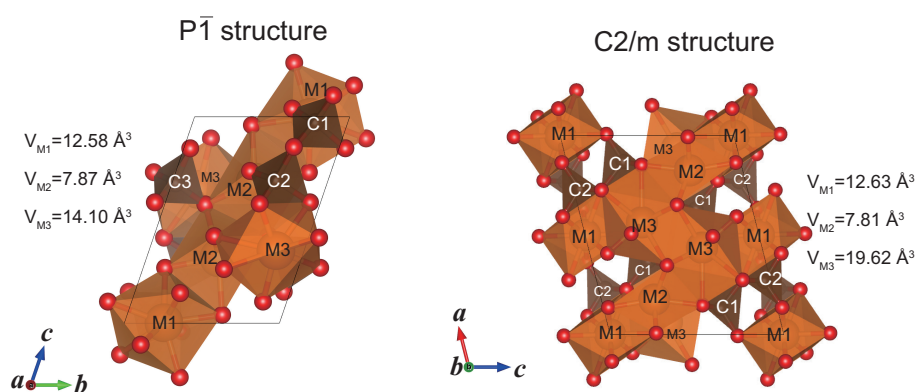
2. Results

2.1. Calculation of $MgCO_3$ Polymorphs under Pressure

First, we optimized the structural parameters of $R\bar{3}c$, $P\bar{1}$, and $C2/m$ structures of $MgCO_3$ polymorphs and confirmed that our calculations are consistent with previously reported results (Table 1) [11,12]. In particular, the coordination number (CN) of all Mg sites is six in $R\bar{3}c$ structure, whereas $P\bar{1}$ and $C2/m$ structures contain three different crystallographic Mg sites (Figure 1). Some of the CNs of Mg in $P\bar{1}$ and $C2/m$ structures are larger than six ($P\bar{1}$: $CN_{M1} = 8$, $CN_{M2} = 6$, $CN_{M3} = 8$; $C2/m$: $CN_{M1} = 8$, $CN_{M2} = 8$, $CN_{M3} = 10$), and thus their polyhedral volumes are significantly larger than that of $R\bar{3}c$ ($V_M = 9.0\sim 12.0 \text{ \AA}^3$) (Figure 1).

Table 1. Optimized structural parameters of $P\bar{1}$ and $C2/m$ phases of $MgCO_3$ polymorphs.

$P\bar{1}$ structure at 100 GPa				
a = 5.178 Å, b = 5.206 Å, c = 7.242 Å, $\alpha = 69.85^\circ$, $\beta = 81.64^\circ$, $\gamma = 78.04^\circ$				
(Pickard and Needs [12]: a = 5.211 Å, b = 5.238 Å, c = 7.268 Å, $\alpha = 70.030^\circ$, $\beta = 81.904^\circ$, $\gamma = 78.272^\circ$ at 100 GPa)				
Atom	Wyckoff position	Atomic coordinates		
		x	y	z
Mg1(M1)	2i	0.7414	0.2541	0.0022
Mg2(M2)	2i	0.5669	0.4731	0.3143
Mg3(M3)	2i	0.0636	0.1784	0.6501
C1	2i	0.2237	0.2078	0.0295
C2	2i	0.0812	0.3351	0.3092
C3	2i	0.4398	0.9790	0.3231
O1	2i	0.1277	0.1522	0.8965
O2	2i	0.0086	0.2930	0.1470
O3	2i	0.8794	0.3896	0.4232
O4	2i	0.3461	0.9572	0.1548
O5	2i	0.3752	0.3872	0.9623
O6	2i	0.2030	0.0682	0.4149
O7	2i	0.2249	0.5252	0.2622
O8	2i	0.5465	0.7397	0.4278
O9	2i	0.6110	0.1433	0.2692
$C2/m$ structure at 120 GPa				
a = 8.0417 Å, b = 6.4468 Å, c = 6.8273 Å, $\beta = 103.84^\circ$				
(Oganov et al. [11]: a = 8.0945 Å, b = 6.4881 Å, c = 6.8795 Å, $\beta = 103.98^\circ$ at 120 GPa)				
Atom	Wyckoff position	Atomic coordinates		
		x	y	z
Mg1(M1)	4g	0.0000	0.7536	0.0000
Mg2(M2)	4i	0.3229	0.5000	0.6975
Mg3(M3)	4i	0.9353	0.5000	0.6555
C1	8j	0.3701	0.3214	0.3273
C2	4i	0.2315	0.5000	0.0363
O1	4i	0.0926	0.5000	0.8961
O2	8j	0.3490	0.1665	0.4299
O3	8j	0.5081	0.3095	0.2675
O4	4i	0.3661	0.5000	0.9729
O5	4i	0.3522	0.5000	0.4276
O6	8j	0.2253	0.3320	0.1595

**Figure 1.** Optimized structures and polyhedral volumes (M1, M2, and M3 sites) of $P\bar{1}$ and $C2/m$ $MgCO_3$ polymorphs at 120 GPa.

2.2. Structure Modeling of $(Mg_{0.833}Fe_{0.167})CO_3$

For the atomic configuration of Fe in $(Mg,Fe)CO_3$, we selected the lowest enthalpy configuration of Fe in the cell. In particular, we used the $2 \times 2 \times 1$ supercell of the conventional $R\bar{3}c$ structure, and replaced four Mg with Fe atoms (Figure 2) to avoid the generation of an FeO_6 octahedral layer.

Consequently, there was almost no site preference for Fe configurations in the $R\bar{3}c$ -type structure because all Mg sites in the $R\bar{3}c$ structure have a CN of six with a Wyckoff $6b$ position. It should be noted that we retain the same crystal structure notations for $(\text{Mg}_{0.833}\text{Fe}_{0.167})\text{CO}_3$ as those of MgCO_3 though the symmetry (space group) of $(\text{Mg}_{0.833}\text{Fe}_{0.167})\text{CO}_3$ polymorphs are changed to $P1$ (no symmetry) because of the incorporation of Fe.

In the $P\bar{1}$ structure, there are three independent Mg positions (Figure 1, Table 1); in addition, we confirmed that the structure with Fe in the M3 position shows the lowest enthalpy in the HS state structures, whereas Fe in the M2 position is the most stable in the LS state structures (Figure 3). Owing to the relatively larger ionic radius of HS-Fe, the structure with a large polyhedral volume ($V_{M3} = 14.10 \text{ \AA}^3$ at 100 GPa) is most stable, whereas, for LS-Fe, the structure with the smallest polyhedral volume ($V_{M2} = 7.87 \text{ \AA}^3$ at 100 GPa) is most stable (Figure 2).

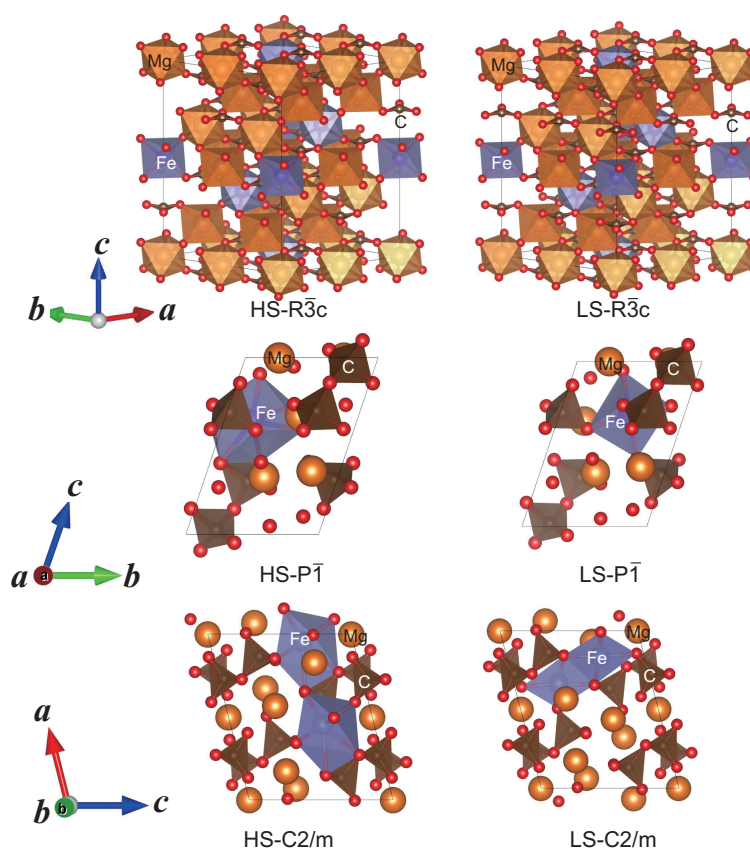


Figure 2. Structural models used for $(\text{Mg}_{0.833}\text{Fe}_{0.167})\text{CO}_3$ polymorphs.

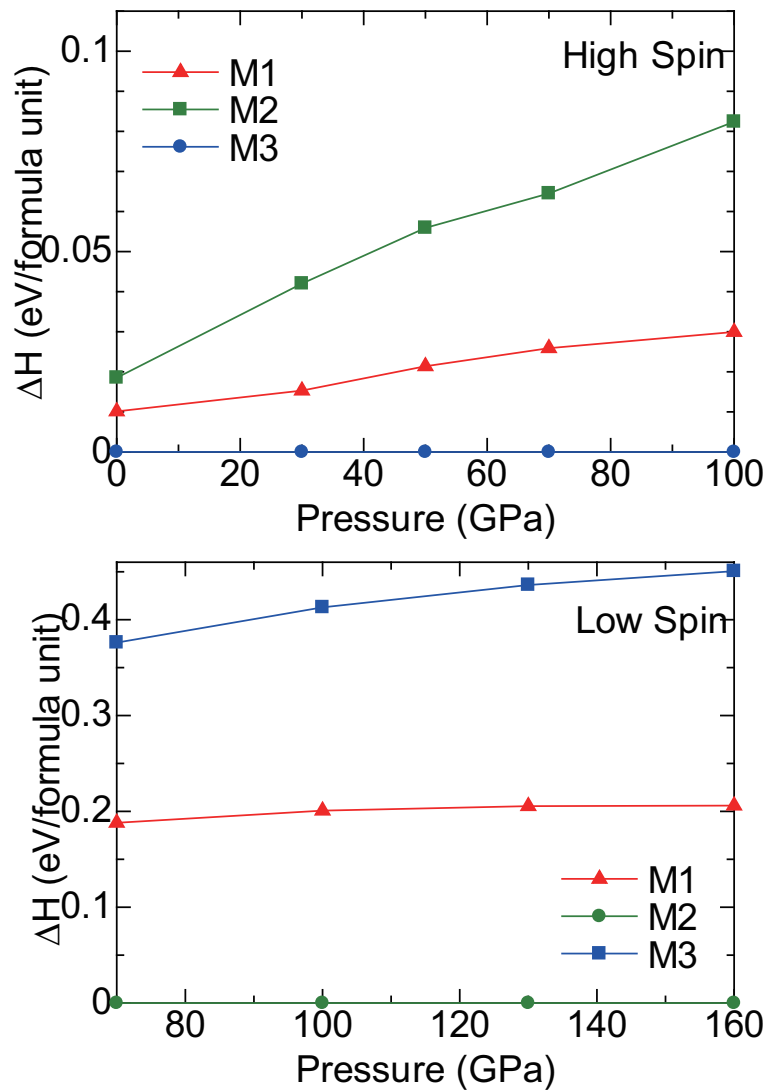


Figure 3. Enthalpies of $P\bar{1}-(Mg_{0.833},Fe_{0.167})CO_3$ structures with respect to the lowest enthalpy configuration.

A similar trend was observed for site preference of Fe in the $C2/m$ crystal structure, wherein HS-Fe atom is the most stable at the M3 site, which has the largest polyhedral volume, whereas LS-Fe atom is most stable at the M2 site leading to the lowest enthalpy (Figure 4).

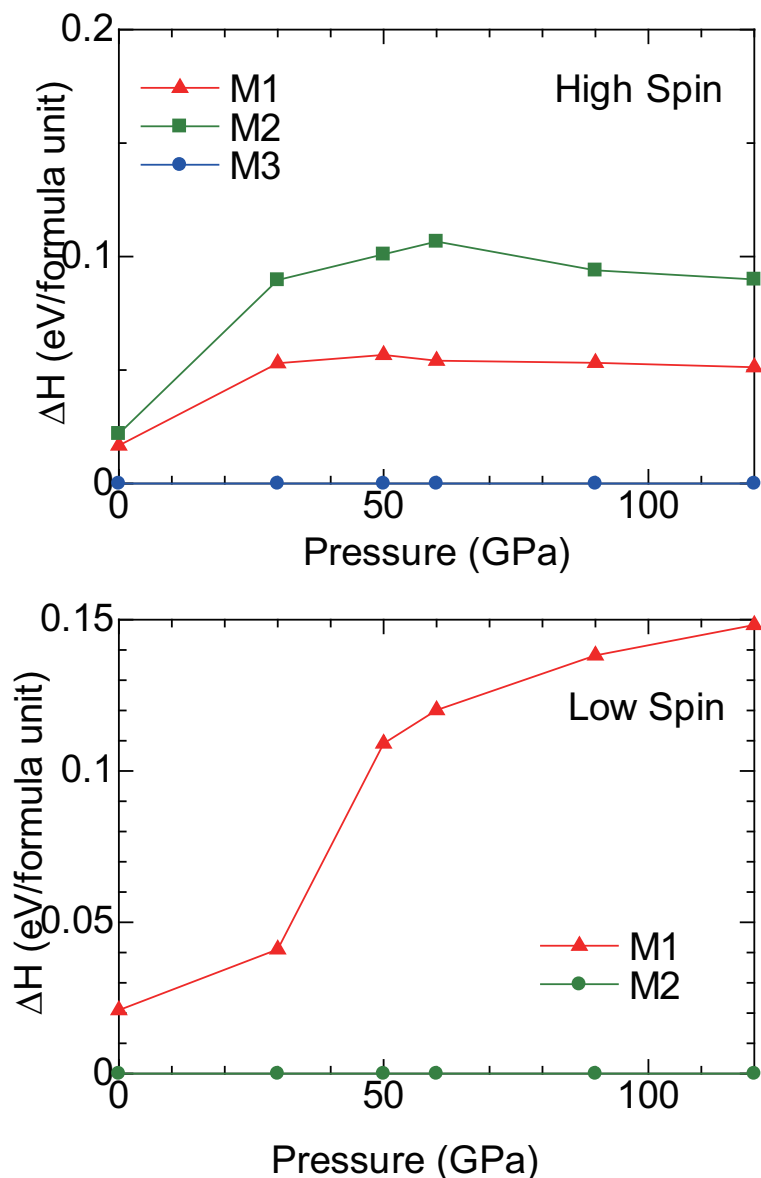


Figure 4. Enthalpies of $C2/m$ - $(Mg_{0.833}Fe_{0.167})CO_3$ structures with respect to the lowest enthalpy configurations. Calculations reveal that the structure with LS-Fe atoms at M3 sites was highly unstable.

2.3. High Pressure Transitions of $MgCO_3$ and $(Mg_{0.833}Fe_{0.167})CO_3$

We have calculated the enthalpy of $MgCO_3$ and $(Mg_{0.833}Fe_{0.167})CO_3$ with $R\bar{3}c$, $P\bar{1}$, and $C2/m$ structures. Figure 5a shows the enthalpy of $MgCO_3$ relative to that of the $C2/m$ phase based on LDA. $MgCO_3$ -magnesite transforms into $P\bar{1}$ phase at 60 GPa, and the $C2/m$ phase is stable above 80 GPa. In contrast, calculations in previous studies indicate the stability of the $P\bar{1}$ phase between 85–101 GPa, and that of the $C2/m$ phase between 101–144 GPa based on GGA [12]. It is typically known that LDA/GGA leads to overestimation/underestimation of the bond strength; therefore, the volume calculated using LDA is usually smaller than that using GGA. Our calculated transition pressures for $MgCO_3$ obtained using LDA are 10–15 GPa lower than those obtained using GGA; however, these GGA results are consistent with previously reported GGA results (Table 2) [12]. Hereafter, in our study, we use LDA results to investigate the stability of ferromagnesite. Nevertheless, it should be noted that the difference of about 10–15 GPa in the transition pressures between LDA and GGA results is typical, and thus, it provides lower and upper bounds for the transition pressures, respectively.

Table 2. Comparison between previously reported calculation results for high-pressure transition of MgCO_3 and those obtained in this study.

	GGA[12]	GGA (This Study)	LDA (This Study)
$R\bar{3}c \rightarrow P\bar{1}$	85	85	62
$P\bar{1} \rightarrow C2/m$	101	95	80
$C2/m \rightarrow P2_12_12_1$	144	145	130

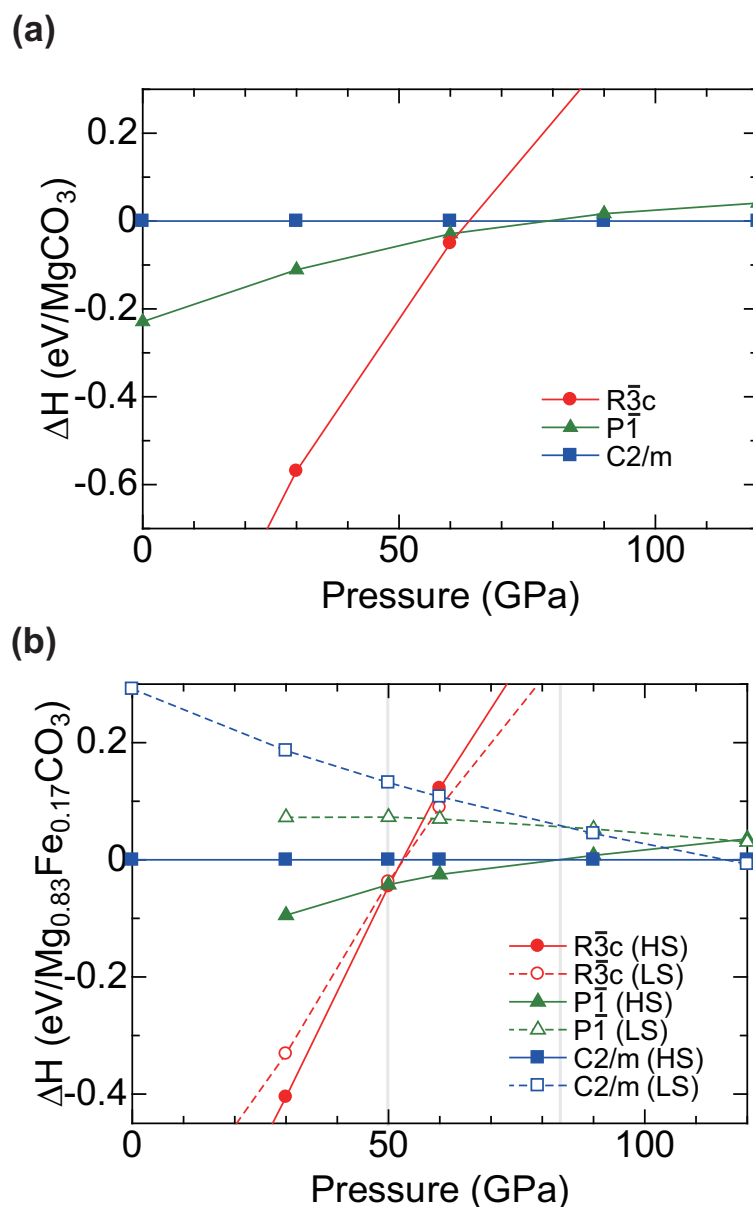


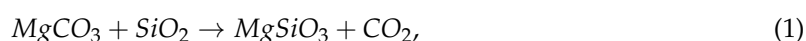
Figure 5. (a) Relative enthalpies of MgCO_3 polymorphs with respect to that of the $C2/m$ phase. These calculations are based on the LDA method. (b) Relative enthalpies of $(\text{Mg}_{0.833}\text{Fe}_{0.167})\text{CO}_3$ under pressure with respect to that of the HS- $C2/m$ phase. These calculations are based on the LDA+ U_{ic} method.

Figure 5b shows the relative enthalpies of ferromagnesite $(\text{Mg}_{0.833}\text{Fe}_{0.167})\text{CO}_3$ and those of its high-pressure candidate phases with respect to the HS- $C2/m$ phase obtained using the LDA+U method. The spin crossover of ferromagnesite (from HS- $R\bar{3}c$ to LS- $R\bar{3}c$) occurs at ~ 50 GPa which is consistent with previously reported calculations [22]. However, the HS- $P\bar{1}$ phase has a lower enthalpy than LS-ferromagnesite above ~ 50 GPa. In addition, the HS- $C2/m$ phase has a slightly lower enthalpy than

that of the HS- $P\bar{1}$ phase above about 80 GPa, and the former is stable up to about 120 GPa, suggesting that no spin crossover is expected under lower mantle pressure conditions. This high stability of the HS state in $P\bar{1}$ and $C2/m$ phases can be attributed to the large polyhedral volumes due to Fe^{2+} in these structures (Figures 1 and 2). However, the energy differences between HS and LS states are relatively small (~ 0.03 eV, equivalent to ~ 350 K) in the $P\bar{1}$ and $C2/m$ phases above 100 GPa. Therefore, there is still a possibility that the high-pressure transition sequence changes or spin crossover occurs around 100 GPa for above-ambient temperature conditions.

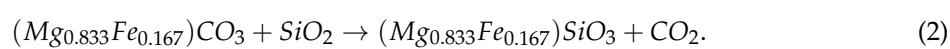
3. Discussion

Carbonate minerals are expected to exist in the subducting cold slabs. Because SiO_2 is one of the most abundant components in a subducting slab, it has been previously indicated that a reaction between $MgCO_3$ and SiO_2 can occur in deeply subducted slabs [8]. We calculated enthalpies of the following chemical reactions to investigate the relative stability of carbonate phases compared with the mantle mineral phases:



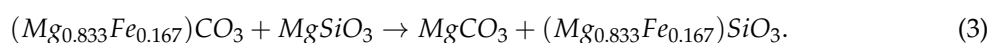
wherein the high pressure phase of CO_2 corresponds to the tetragonal $I4\bar{2}d$ phase [11], SiO_2 is stishovite, and the $CaCl_2$ -type structure below and above 50 GPa, respectively, and $MgSiO_3$ has bridgmanite-type structure. The relative enthalpy curves shown in Figure 6a indicate that the transformation of $MgCO_3$ and SiO_2 into $MgSiO_3$ -bridgmanite along with CO_2 formation is unfavorable, which is consistent with the results reported in previous studies [11,12].

Then, we calculated the reaction between $(Mg_{0.833}Fe_{0.167})CO_3$ and SiO_2 ,



For the calculation of enthalpy of $(Mg_{0.833}Fe_{0.167})SiO_3$, we used the supercell of bridgmanite containing 60 atoms with high spin Fe^{2+} at A sites [24]. Although both Fe^{2+} and Fe^{3+} have been observed in bridgmanite, ferric iron Fe^{3+} content in bridgmanite strongly correlates with the concentration of Al in bridgmanite [25]. In addition, the spin crossover of Fe^{2+} from HS to LS at an A site has not been theoretically shown at lower mantle pressure conditions (e.g., [26]). Moreover, the enthalpy of HS- $(Mg_{0.833}Fe_{0.167})SiO_3$ -bridgmanite plus CO_2 is higher than that of the Fe-bearing carbonate mineral plus SiO_2 up to ~ 120 GPa, which also suggests that decomposition of $(Mg_{0.833}Fe_{0.167})CO_3$ -carbonate phases is unfavorable under lower mantle pressure conditions (Figure 6a).

Finally, we also investigated the stability of Fe^{2+} between bridgmanite and carbonate minerals by the following Fe exchange reaction,



In the case of $R\bar{3}c$ structures, the enthalpy of the mixture of $(Mg,Fe)CO_3$ and $MgSiO_3$ is higher than that of $MgCO_3$ and $(Mg,Fe)SiO_3$ (Figure 6b), which indicates that Fe^{2+} is more stable in bridgmanite than in $(Mg,Fe)CO_3$. HS- Fe^{2+} is more stable at the A site of bridgmanite because the polyhedral volume of the A site of the bridgmanite ($16\text{--}21 \text{ \AA}^3$) is significantly larger than those of ferromagnesite ($7\text{--}12 \text{ \AA}^3$). However, the HS- Fe^{2+} is more stable in $P\bar{1}$ and $C2/m$ structures because HS- Fe^{2+} can be well accommodated at the sites with large polyhedral volumes in these phases.

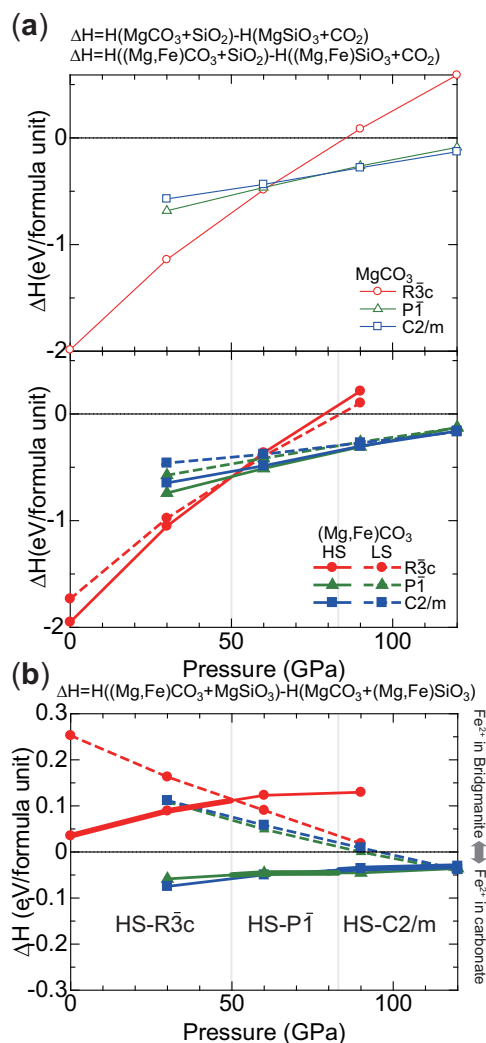


Figure 6. (a) The thin lines correspond to the relative enthalpy of $\text{MgCO}_3 + \text{SiO}_2$ with respect to $\text{MgSiO}_3\text{-bridgmanite} + \text{CO}_2$. The full/dashed lines indicate the relative enthalpy of the HS/LS- $(\text{Mg}_{0.833}\text{Fe}_{0.167})\text{CO}_3 + \text{SiO}_2$ with respect to the HS- $(\text{Mg}_{0.833}\text{Fe}_{0.167})\text{SiO}_3\text{-bridgmanite} + \text{CO}_2$. (b) The relative stability of $(\text{Mg}_{0.833}\text{Fe}_{0.167})\text{CO}_3 + \text{MgSiO}_3\text{-bridgmanite}$ and HS- $(\text{Mg}_{0.833}\text{Fe}_{0.167})\text{SiO}_3\text{-bridgmanite} + \text{MgCO}_3$ as a function of pressure. The thick lines indicate the enthalpies of the reactions containing the lowest enthalpy phase of $(\text{Mg,Fe})\text{CO}_3$ as shown in Figure 5b.

4. Conclusions

In this study, we calculated the enthalpy of ferromagnesite $(\text{Mg}_{0.833}\text{Fe}_{0.167})\text{CO}_3$ to investigate the effect of Fe on the stability of high-pressure phases of magnesite. Our enthalpy calculations suggest that $(\text{Mg}_{0.833}\text{Fe}_{0.167})\text{CO}_3$ undergoes phase transition from the HS- $R\bar{3}c$ structure to the HS- $P\bar{1}$ structure at 50 GPa, and to the HS- $C2/m$ structure above 80 GPa at static 0 K conditions. Therefore, no spin transition in $(\text{Mg}_{0.833}\text{Fe}_{0.167})\text{CO}_3$ is expected under the lower mantle pressure conditions. This result also indicates that the effect of Fe on the transition pressure of high-pressure phases of ferromagnesite is not significant.

Furthermore, the calculated enthalpy relationship suggests that the high-pressure phase of ferromagnesite plus SiO_2 does not decompose even up to pressures of ~ 120 GPa. In addition, the enthalpy of the Fe^{2+} exchange reaction between magnesite and bridgmanite shows a weaker preference in the high-pressure carbonate phases than in bridgmanite under deep lower mantle pressure conditions.

5. Methods

5.1. First Principles Calculation

We performed first principles calculation based on the density functional theory (DFT) [27,28] for the determination of the relative stability of $(\text{Mg}_{0.833}\text{Fe}_{0.167})\text{CO}_3$ ferromagnesite and its possible high-pressure phases. We used the norm-conserving pseudopotentials [29] for Mg and Si, which have also been used extensively in previous studies e.g., [30]. In contrast, we used ultrasoft pseudopotentials for Fe, C, and O [31,32]. The electronic wave functions are expanded into plane-waves with a kinetic cutoff of 50 Ry. The irreducible Brillouin zone of $R\bar{3}c$ (ferromagnesite), $P\bar{1}$, and $C2/m$ phases were sampled on $2 \times 2 \times 2$, $4 \times 4 \times 4$, and $4 \times 4 \times 4$ Monkhorst-Pack meshes with shifted grids, respectively [33]. The associated k-point sampling and kinetic energy cutoff are sufficiently converged within 0.001 eV/ $(\text{Mg}_{0.833}\text{Fe}_{0.167})\text{CO}_3$. All structure parameters of MgCO_3 and $(\text{Mg}_{0.833}\text{Fe}_{0.167})\text{CO}_3$ were fully relaxed at static 0 K and in the range of 0–120 GPa via the damped variable cell-shape molecular dynamics method implemented using a Quantum-espresso code until residual forces were less than 1.0×10^{-4} Ry/a.u. (a.u. = atomic unit) [34].

The number of atoms calculated in the MgCO_3 cells are 30 for the $R\bar{3}c$ (Wyckoff positions of Mg, C, and O are $6b$, $6a$, and $18e$, respectively) and $P\bar{1}$ structures, whereas they are 60 for the $C2/m$ structure (Wyckoff positions of $P\bar{1}$ and $C2/m$ structures are listed in Table 1). For the $(\text{Mg}_{0.833}\text{Fe}_{0.167})\text{CO}_3$ composition, we constructed a supercell containing 120, 60, and 30 atoms for the $R\bar{3}c$, $P\bar{1}$, and $C2/m$ structures, respectively (Figure 2).

5.2. LDA+ U_{ic} Calculation

Because LDA and GGA typically fail to accurately determine the phase relationship of Fe-bearing mineral oxides owing to the large on-site Coulomb interactions of $3d$ Fe electrons, in this study, we performed calculations based on LDA with Hubbard U correction, where U values were determined using an internally consistent method (U_{ic} , Figure 7) [23]. This method has been successfully applied for mantle mineral stability calculations [24,35,36]. The U_{ic} parameters for HS state of $(\text{Mg,Fe})\text{CO}_3$ are obtained in the range of 3.5–4.0 eV, except for ferromagnesite (HS- $R\bar{3}c$), for which they are higher than those reported in a previous study [22]. The large U_{ic} of the HS ferromagnesite could be attributed to the Fe atom occupying the small octahedral site in the $R\bar{3}c$ structure. In contrast, the U_{ic} parameters of the LS state are in the range of 5.0–7.0 eV.

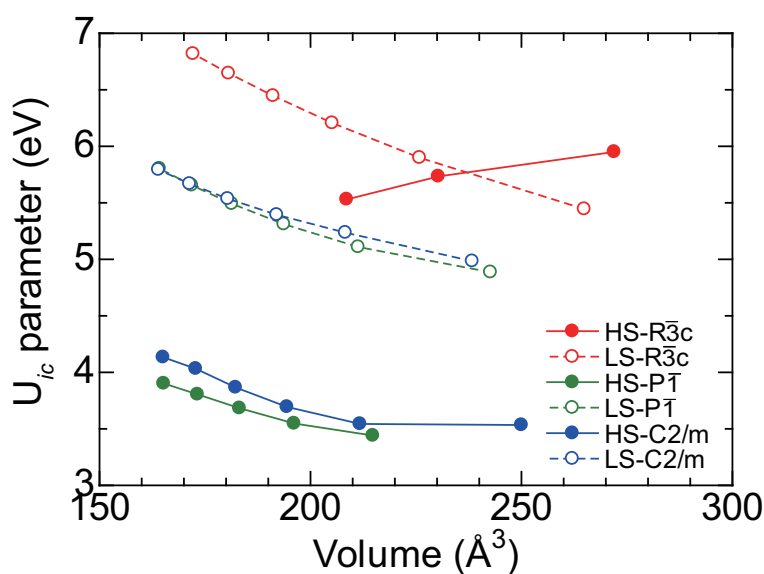


Figure 7. Volume (per 30 atoms) dependence of U_{ic} parameters for $(\text{Mg,Fe})\text{CO}_3$.

Author Contributions: J.T. and R.N. conducted the first principles calculation. All authors analyzed the results. J.T. and T.T., J.T. drafted the manuscript. All authors have read and agreed to the published version of the manuscript.

Funding: The research was supported in part by Grants-In-Aid for Scientific Research from the Japan Society for the Promotion of Science (No. JP15H05834 for J.T. and T.T. and No. JP19H01994 for J.T.). In addition, it was also supported by MEXT as “Exploratory Challenge on Post-K computer” (Challenge of Basic Science - Exploring Extremes through Multi-Physics and Multi-Scale Simulations).

Acknowledgments: We are grateful to two anonymous reviewers who helped to improve the manuscript.

Conflicts of Interest: The authors declare no conflict of interest.

References

1. Merlini, M.; Crichton, W.A.; Hanfland, M.; Gemmi, M.; Muller, H.; Kupenko, I.; Dubrovinsky, L. Structures of dolomite at ultrahigh pressure and their influence on the deep carbon cycle. *Proc. Natl. Acad. Sci. USA* **2012**, *109*, 13509–13514. [[CrossRef](#)] [[PubMed](#)]
2. Boulard, E.; Gloter, A.; Corgne, A.; Antonangeli, D.; Auzende, A.; Perrillat, J.; Guyot, F.; Fiquet, G. New host for carbon in the deep Earth. *Proc. Natl. Acad. Sci. USA* **2011**, *108*, 5184–5187. [[CrossRef](#)] [[PubMed](#)]
3. Biellmann, C.; Gillet, P.; Guyot, F.; Peyronneau, J.; Reynard, B. Experimental evidence for carbonate stability in Earth’s lower mantle. *Earth Planet. Sci. Lett.* **1993**, *118*, 31–41. [[CrossRef](#)]
4. Gillet, P. Stability of magnesite (MgCO₃) at mantle pressure and temperature conditions: A raman spectroscopic study. *Am. Miner.* **1993**, *78*, 1328–1331.
5. Fiquet, G.; Guyot, F.; Kunz, M.; Matas, J.; Andraut, D.; Hanfland, M. Structural refinements of magnesite at very high pressure. *Am. Miner.* **2002**, *87*, 1261–1265.
6. Shatskiy, A.; Litasov, K.D.; Palyanov, Y.N.; Ohtani, E. Phase relations on the K₂CO₃-CaCO₃-MgCO₃ join at 6 GPa and 900–1400 °C: Implications for incipient melting in carbonated mantle domains. *Am. Miner.* **2016**, *101*, 437–447. [[CrossRef](#)]
7. Isshiki, M.; Irifune, T.; Hirose, K.; Ono, S.; Ohishi, Y.; Watanuki, T.; Nishibori, E.; Tanaka, M.; Sakata, M. Stability of magnesite and its high-pressure form in the lowermost mantle. *Nature* **2004**, *427*, 60–63. [[CrossRef](#)]
8. Maeda, F.; Ohtani, E.; Kamada, S.; Sakamaki, T.; Hirao, N.; Ohishi, Y. Diamond formation in the deep lower mantle: A high-pressure reaction of MgCO₃ and SiO₂. *Sci. Rep.* **2017**, *7*, 40602. [[CrossRef](#)]
9. Palyanov, Y. N. Mantle-slab interaction and redox mechanism of diamond formation. *Proc. Natl. Acad. Sci. USA* **2013**, *110*, 20408–20413. [[CrossRef](#)]
10. Kelemen, P.B.; Manning, C.E. Reevaluating carbon fluxes in subduction zones, what goes down, mostly comes up. *Proc. Natl. Acad. Sci. USA* **2015**, *112*, E3997–E4006. [[CrossRef](#)]
11. Oganov, A.R.; Ono, S.; Ma, Y.; Glass, C.W.; Garcia, A. Novel high-pressure structures of MgCO₃, CaCO₃ and CO₂ and their role in Earth’s lower mantle. *Earth Planet. Sci. Lett.* **2008**, *273*, 38–47. [[CrossRef](#)]
12. Pickard, C.; Needs, R.J. Structures and stability of calcium and magnesium carbonates at mantle pressures. *Phys. Rev. B* **2015**, *91*, 104101. [[CrossRef](#)]
13. Franzolin, E.; Schmidt, M.W.; Poli, S. Ternary Ca-Fe-Mg carbonates: subsolidus phase relations at 3.5 GPa and a thermodynamics solid solution model including order/disorder. *Contrib. Miner. Petrol.* **2011**, *161*, 213–227. [[CrossRef](#)]
14. Liu, J.; Lin, J.-F.; Prakapenka, V.B. Ferromagnesite as a potential deep-mantle carbon carrier. *Sci. Rep.* **2015**, *5*, 7940. [[CrossRef](#)]
15. Solomatova, N.V.; Asimow, P.D. First-principles calculations of high-pressure iron-bearing monoclinic dolomite and single-cation carbonates with internally consistent Hubbard U. *Phys. Chem. Miner.* **2018**, *45*, 293–302. [[CrossRef](#)]
16. Boulard, E.; Menguy, N.; Auzende, A.L.; Bureau, H.; Antonangeli, D.; Corgne, A.; Morard, G.; Siebert, J.; Perrillat, J.P.; Guyot, F.; et al. Experimental investigation of the stability of Fe-rich carbonates in the lower mantle. *J. Geophys. Res.* **2012**, *117*, B02208. [[CrossRef](#)]
17. Lavina, B.; Dera, P.; Downs, R.T.; Prakapenka, V.; Rivers, M.; Sutton, S.; Nicol, M. Siderite at lower mantle conditions and the effects of the pressure-induced spin-apiring transition. *Geophys. Res. Lett.* **2009**, *36*, L23306. [[CrossRef](#)]

18. Lavina, B.; Dera, P.; Downs, R.T.; Yang, W.; Sinogeikin, S. Meng, Y.; Shen, G.; Schiferl, D. Structure of siderite FeCO_3 to 56 GPa and hysteresis of its spin-pairing transition. *Phys. Rev. B* **2010**, *82*, 064110. [[CrossRef](#)]
19. Mattila, A.; Pylkkanen, T.; Rueff, J.-P.; Huotari, S.; Vanko, G.; Hafland, M.; Lehtinen, M.; Hamalainen, K. Pressure induced magnetic transition in siderite FeCO_3 studied by x-ray emission spectroscopy. *J. Phys. Condens. Matter* **2007**, *19*, 386206. [[CrossRef](#)]
20. Farfan, G.; Wang, S.; Ma, H.; Caracas, R.; Mao, W.L. Bonding and structural changes in siderite at high pressure. *Am. Miner.* **2012**, *97*, 1421. [[CrossRef](#)]
21. Lin, J.-F.; Liu, J.; Jacobs, C.; Prakapenka, V.B. Vibrational and elastic properties of ferromagnesite across the electronic spin-pairing transition of iron. *Am. Miner.* **2012**, *97*, 583. [[CrossRef](#)]
22. Hsu, H.; Huang, S.C. Spin crossover and hyperfine interactions of iron in $(\text{Mg,Fe})\text{CO}_3$ ferromagnesite. *Phys. Rev. B* **2016**, *94*, 060404. [[CrossRef](#)]
23. Cococcioni, M.; de Gironcoli, S. Linear response approach to the calculation of the effective interaction parameters in the LDA+U method. *Phys. Rev. B* **2005**, *71*, 035105. [[CrossRef](#)]
24. Wang, X.; Tsuchiya, T.; Hase, A. Computational support for a pyrolitic lower mantle containing ferric iron. *Nat. Geosci.* **2015**, *8*, 556–560. [[CrossRef](#)]
25. McCammon, C. Perovskite as a possible sink for ferric iron in the lower mantle. *Nature* **1997**, *387*, 694–696. [[CrossRef](#)]
26. Zhang, F.; Oganov, A.R. Valence state and spin transitions of iron in Earth's mantle silicates. *Earth Planet. Sci. Lett.* **2006**, *249*, 436–443. [[CrossRef](#)]
27. Hohenberg, P.; Kohn, W. Inhomogeneous electron gas. *Phys. Rev.* **1964**, *136*, B864–B871. [[CrossRef](#)]
28. Kohn, W.; Sham, L.J. Self-consistent equations including exchange and correlation effects. *Phys. Rev.* **1965**, *140*, A1133–A1138. [[CrossRef](#)]
29. Troullier, N.; Martins, J.L. Efficient pseudopotential for plane wave calculations. *Phys. Rev. B* **1991**, *43*, 1993–2006. [[CrossRef](#)]
30. Tsuchiya, T.; Tsuchiya, J.; Umemoto, K.; Wentzcovitch, R.M. Phase transition in MgSiO_3 perovskite in the earth's lower mantle. *Earth Planet. Sci. Lett.* **2004**, *224*, 241–248. [[CrossRef](#)]
31. Ichikawa, H.; Tsuchiya, T.; Tange, Y. The P-V-T equation of state and thermodynamic properties of liquid iron. *J. Geophys. Res. Solid Earth* **2013**, *119*, 240–252. [[CrossRef](#)]
32. Vanderbilt, D. Soft self-consistent pseudopotentials in a generalized eigenvalue formalism. *Phys. Rev. B* **1990**, *41*, 7892–7895. [[CrossRef](#)]
33. Monkhorst, H.J.; Pack, J.D. Special points for Brillouin-zone integrations. *Phys. Rev. B* **1976**, *13*, 5188–5192. [[CrossRef](#)] [[PubMed](#)]
34. Giannozzi, P.; Baroni, S.; Bonini, N.; Calandra, M.; Car, R.; Cavazzoni, C.; Ceresoli, D.; Chiarotti, G.L.; Cococcioni, M.; Dabo, I.; et al. Quantum ESPRESSO: A modular and open-sourcesoftware project for quantum simulations of materials. *J. Phys. Condens. Matter* **2009**, *21*, 395502. [[CrossRef](#)]
35. Tsuchiya, T.; Wentzcovitch, R.M.; da Silva, C.R.S.; de Gironcoli, S. Spin transition in magnesiowustite in earth's lower mantle. *Phys. Rev. Lett.* **2006**, *96*, 198501. [[CrossRef](#)]
36. Fukui, H.; Tsuchiya, T.; Baron, A.Q.R. Lattice dynamics calculations for ferropericlase with internally consistent LDA+U method. *J. Geophys. Res.* **2012**, *117*, B12202. [[CrossRef](#)]

